Numerical Investigation on the Influence of the Fuel on the Performance of a Laboratory Combustor

Pedro Daniel Canuto Rijo

pedro.c.rijo@tecnico.ulisboa.pt

Instituto Superior Técnico, Universidade de Lisboa, Portugal

July 2020

Abstract

In this work, numerical simulations were performed to study the fuel flexibility of a small-scale combustor operating in the flameless combustion mode. The combustor geometrical characteristics and the operating conditions, such as thermal power and equivalence ratio (φ), were kept constant for all fuels studied. All calculations were performed using the commercial code *Ansys Fluent 18* with the realizable k-ε model for turbulence closure and the eddy dissipation concept (EDC) for combustion modeling. The studied fuels were: methane, biogas, ethanol, syngas and mixtures of CH_4/NH_3 and H_2/NH_3. The numerical results show that for a preheated air temperature of 900 K and φ = 0.5, flameless combustion can be obtained for all fuels except syngas. This fuel has a non-uniform temperature field combined with rapid oxygen and fuel consumption, which suggests the presence of a flame front. In the CH_4/NH_3 and H_2/NH_3 mixtures, the flameless combustion can be performed for φ ≤ 1. In the fuel-rich condition (φ = 1.2), the numerical results suggest the presence of a flame front for both mixtures. Flameless combustion is characterized by low NO_x emissions (< 15 ppm) for nitrogen-free fuels. However, the NO_x concentration obtained in the CH_4/NH_3 and H_2/NH_3 mixtures is above 800 ppm for this combustion mode, which suggests a need to optimize flameless combustion for ammonia-rich fuels.

Keywords: combustor flexibility, flameless combustion, biogas, ethanol, methane, syngas, ammonia combustion

1. Introduction

Since the first industrial revolution until today, global economic growth has been based on the aggressive consumption of fossil fuels and their derivatives, which has led to an increase in the concentration of greenhouse gases (GHG) in the atmosphere. This consequence has contributed to an increase in the Earth's average temperature and acceleration of climate change. Around 195 countries have agreed to limit this temperature increase of 1.5 ºC and have established a set of initiatives included in the Paris Agreement to achieve this aim [1]. One of the main initiatives is the strong reduction in GHG emissions, especially carbon dioxide (CO_2), carbon monoxide (CO), nitrogen oxides (NO_x), methane (CH_4) and floured gases.

The reduction of GHG emissions can be achieved using flameless combustion technology in the power generation and industrial sectors. The flameless combustion, also known by moderate or intense low-oxygen dilution (MILD) combustion, colorless distribution combustion (CDC) or high temperature air combustion (HiTAC), is a mature technology and has been successfully applied in the metallurgi-

cal industries. This technology allows an improvement of 30% in thermal efficiency, which means a reduction in fuel consumption and CO_2 emission, as well as a 70% reduction in NO_x emission [2]. Furthermore, this technology makes it possible to burn fuels with low heating value instead of conventional modes where there are flame instability, flashback and blow-off phenomena.

The use of alternative fuels to natural gas, such as biogas [3], syngas [4], ethanol [5] and ammonia [6], has been studied applying this technology although the combustor characteristics and the operating conditions used differ between them. These differences do not allow to understand if a flameless combustor has the flexibility to burn different fuels for the same operating conditions. So, the aims of this work are to study numerically the laboratory combustor flexibility to burn a diverse set of fuels for the same operating conditions and to report which combustion mode applied.

2. Numerical Modelling

The furnace investigated in this study is similar to the one used by Rebola *et al.* [7,8]. The combustion chamber is a stainless-steel cylinder with an inner diameter of 150 mm and a length of 300 mm. The burner consists of a central gas gun and a combustion air supply in a conventional double concentric configuration. The burner is placed on top of the combustion chamber and the flue gases are exhausted at the opposite end through a convergent nozzle with a length of 50 mm and an angle of 35º. The simulations were carried out using two-dimensional axisymmetric and unstructured mesh composed by quadrilateral elements. The computational domain used is represented in figure 1.

The governing equations for continuity, energy, momentum, species and chemical reaction are solved in the combustion simulation process by the Favre-average approach. The turbulence model used is a realizable k-ε model. In this model, the two transport equations are deduced mathematically in order to respect the mathematical constraint of the normal Reynolds stress, which sometimes produces results without physical significance when the computational domain has stationary and rotation fluid zones [9].

The species transport model used is the Eddy Dissipation Concept (EDC). According to Rebola *et al.* [8], the EDC is the best model for predicting flameless combustion and allows to use more complex kinetic mechanisms. The In-Situ Adaptative Tabulation (ISAT) method was used to reduce the computational cost of the chemical source term integration for the EDC model.

The Discrete Ordinate (DO) model is used to simulate the radiative heat transfer and the radiative properties of the participating medium are calculated based on the Weight-Sum-of-Grey-Gas (WSGG) model where the emissivity

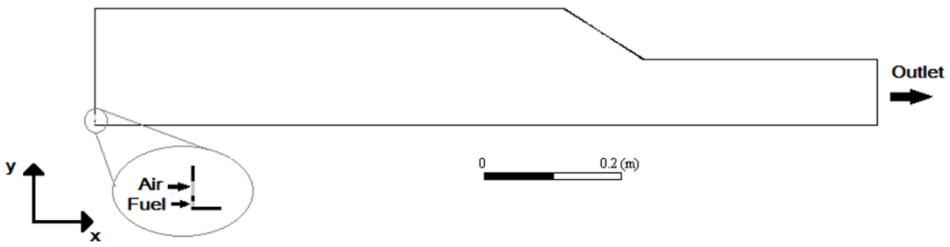

Figure 1 – Computational domain of the combustor

is determined as a function of the local temperature and mass fraction of water vapor and CO_2.

The convergence of the solution for all the simulations carried out was based on the sum of the residuals for each equation and the monitoring of a set of predefined points. In the first part of the convergence criteria, it was defined that the sum of the residues had to be less than 10^{-4} for continuity and species, 5×10^{-6} for radiation and 10^{-6} for the rest. The second convergence criterion is based on monitoring the following variables: axial velocity, temperature and molar fractions of CO_2, CO, H_2 and NH_3 for three different positions in the combustion chamber.

Table 1 – Tested Conditions[a]

Fuel	φ	Air inlet velocity (m/s)	Fuel inlet velocity (m/s)
Methane	0.5	102.1	24.4
Biogas	0.5	101.00	39.74
Ethanol[b]	0.5	95.11	21.60
Syngas	0.5	79.93	89.85
CH_4/NH_3	0.5	97.89	46.22
	2/3	73.42	
	1	48.95	
	1.2	40.79	
H_2/NH_3	0.5	93.98	63.39
	2/3	70.48	
	1	46.99	
	1.2	39.16	

[a]For all conditions: fuel thermal input = 10 kW, fuel inlet temperature = 293 K (except ethanol), air inlet temperature = 773 K, wall temperature = 1173 K. [b]For ethanol: fuel inlet temperature = 423 K.

Table 1 summarizes the tested conditions used in this work and table 2 shows the chemical composition in molar fraction for the mixtures studied. The first condition was studied experimentally and numerically by Rebola *et al.* [7,8] and this allows to study the type of combustion mode which is applied for the remaining fuels. For each fuel, the most suitable kinetic mechanism was applied for the simulation of non-premixed combustion and the operating conditions used.

Table 2 – Chemical composition of the mixtures studied.

Fuel	Composition in molar fraction
Biogas	60%CH_4+40%CO_2
Syngas	40%CO+38%H_2+14%N_2
CH_4/NH_3	20%CH_4+80%NH_3
H_2/NH_3	20%H_2+80%NH_3

3. Results and Discussion

All simulations were carried out using a commercial code *Ansys Fluent 18*. The grid independency study was performed through the comparison of three different meshes composed by 50 000, 79 000 and 114 000 elements, respectively. The results obtained in three meshes show a marginal difference in the temperature field and the CO and NO_x concentration fields. The differences observed between the coarse and fine mesh are less than the uncertainty of the measurement equipment used by Rebola *et al.* [7]. However, the coarse mesh tends to overestimate the temperature and NO_x concentration and to underestimate the CO concentration compared to the values obtained in the other two meshes. Based on this, the grid independence was ensured and the intermediate mesh was used in this work.

Based on previous experimental and numerical studies carried out on this small-scale combustor [7,8] and based on the fundamental knowledge acquired in the literature, the nature of the flow must be explained to better under-

stand the results presented. The momentum of the air jet is strong enough to generate a reverse flow zone that is responsible for the recirculation of the hot flue gases towards the reactant inlet zone. This momentum is also responsible for the dilution of the fuel from the central jet and the oxygen in the entire combustion chamber to allow flameless combustion, see figure 2.

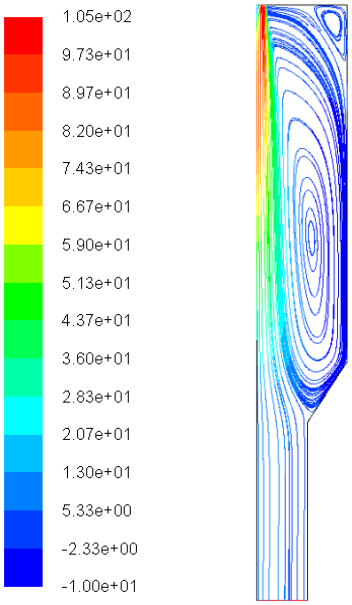

Figure 2 – Streamlines of axial velocity for methane flameless combustion.

3.1 Axial Profiles of the Relevant Parameters for Different Fuels

From figure 3, it is observed that the velocity profiles of methane, biogas and ethanol are similar. Until the position x ≈ 5 mm, there is a slight reduction in velocity and then a progressive velocity increase to the position x ≈ 100 mm. In this point, the maximum velocity is reached and then the velocity decrease until it becomes constant downstream of the point x = 400 mm. The velocity reduction of the fuel jet observed at the beginning occurs because according to equation 1, the temperature increase in that initial region is less than the increase of the jet cross-sectional area.

$$\frac{U_{x_2}}{U_{x_1}} = \frac{A_{x_1}}{A_{x_2}} \cdot \frac{T_{x_2}}{T_{x_1}} \quad (1)$$

The minimum velocity recorded at the point x ≈ 5 mm occurs when the air and fuel jet shear layers merge. From this point, a fuel jet acceleration occurs because the air jet velocity is higher than fuel jet velocity, which performs a momentum transfer to the fuel jet. The acceleration of the central jet also occurs because the temperature increase compensates the increase of the jet cross-sectional area according to equation 1. Downstream of the point x = 100 mm, the jet velocity decreases because the temperature increase of the central jet does not compensate the increase of the jet cross-sectional area, but also due to momentum transfer to the recirculated flue gas, which has a lower velocity compared to the reactants.

In relation to syngas, there is an absence of the first two phases in the velocity profile since the air jet velocity is lower than the fuel jet velocity. Therefore, a gradual reduction in velocity is observed up to the position x ≈ 400 mm, from which the velocity remains constant.

Based on figure 3, it is observed that the temperature profile and the O_2, CO and NO_x concentrations profiles for CH_4, biogas and ethanol have similar behavior. The maximum temperatures differ because the fuels have different adiabatic flame temperatures, with the higher adiabatic flame temperature in ethanol followed by biogas and methane. The maximum temperature, O_2, CO_2 and CO concentrations also differ since the air-fuel ratio and the chemical composition differ from fuel to fuel. According to the available CO data, it is

observed that the onset of CO oxidation occurs for different positions depending on the fuel used and for different CO consumption rates. For ethanol, biogas and CH_4, the onset of CO oxidation takes place between x = 300 mm and x = 350 mm which corresponds to the combustion chamber section where the reduction of the cross-sectional area takes place, see figure 3.

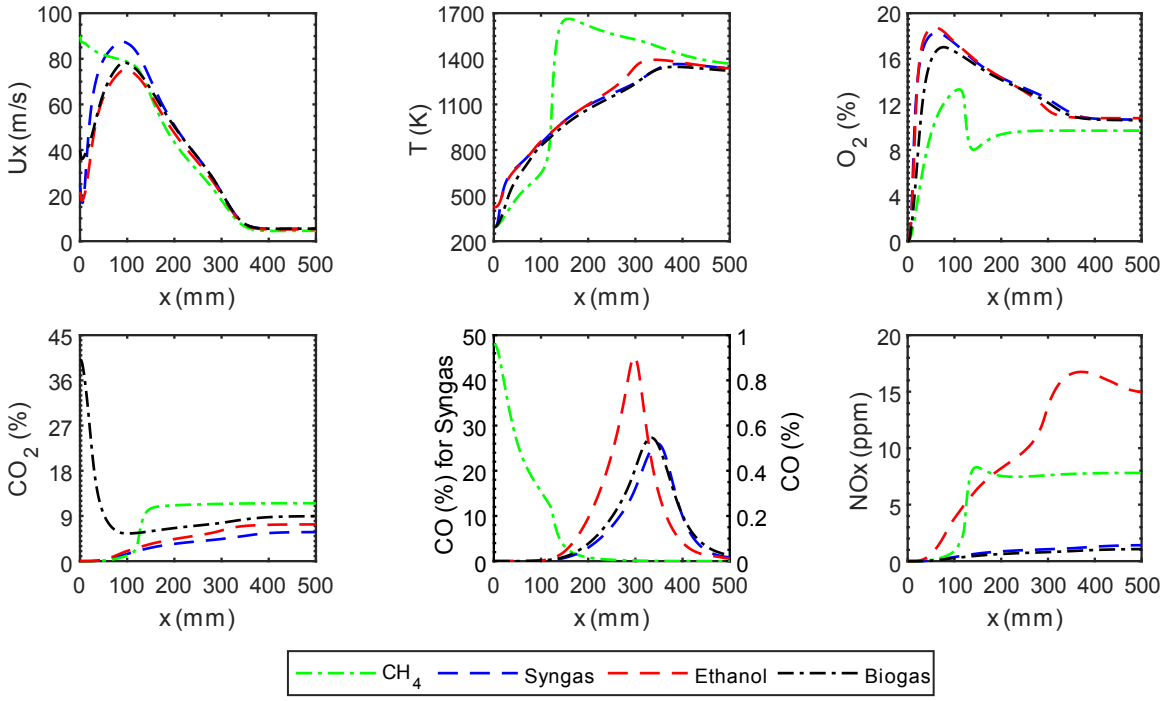

Figure 3 – Axial profiles of velocity, temperature, O_2, CO_2, CO and NO_x concentrations on dry basis for combustion of methane (CH_4), syngas, ethanol and biogas.

In the syngas combustion, it can be seen a rapid increase in temperature and CO_2 concentration from the position x = 110 mm, which is accompanied by a sharp reduction in the concentrations of O_2, CO and H_2, see figure 3. In flameless combustion, the temperature profile is characterized by smooth temperature gradients while in conventional combustion there is a sudden temperature increase followed by a smooth temperature decrease when moving away of the flame front. In syngas, there is an increase of approximately 950 K from the point x = 110 mm to the point x = 160 mm, where the maximum temperature occurs. This sudden temperature increase suggests the appearance of a flame inside the combustion chamber.

Due to the growing interest in ammonia (NH_3) combustion as a carbon-free fuel, the next paragraphs of this section will be dedicated to analyzing and discussing the results obtained in simulations of ammonia mixed with methane or hydrogen. In this work, the influence of the equivalence ratio was studied.

From figure 4, it is observed that the velocity profiles are similar to the methane velocity profile when the equivalence ratio is less than 1. The maximum velocity decreases for $\varphi \leq 1$ because the air mass flow rate decreases when the φ increases, which decreases the momentum transfer to accelerate the central jet. For $\varphi > 1$, the jet velocity is maximum at the injector outlet since the air jet velocity is less than the fuel jet velocity. In this case, there is a

momentum transfer from the fuel jet to the air jet, which tends to slow down the fuel jet velocity.

4. It is expected that the O_2 concentration at the combustor outlet will decrease with equivalence ratio increase and that for stoichiometric and

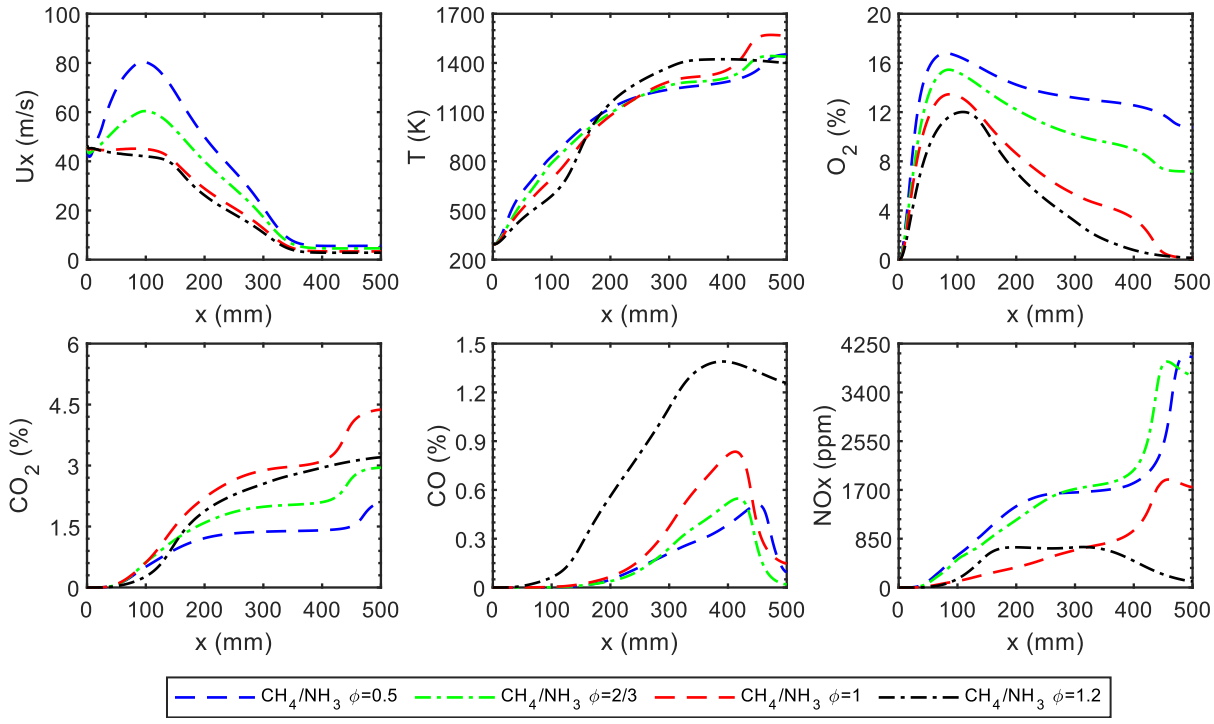

Figure 4 – Axial profiles of velocity, temperature, O_2, CO_2, CO and NO_x for combustion of CH_4/NH_3 mixture.

In figure 4, it is observed that the temperature profiles obtained for mixtures with φ ≤ 1 have a similar behavior to the methane temperature profile. For these mixtures, there is a moderate temperature increase downstream of x = 400 mm, which is also observed in the CO_2 and NO_x concentration profiles and a decrease of O_2 and CO concentrations after this point. For φ = 1.2, a temperature increase of approximately 565 K is observed between the points x = 100 mm and x = 200 mm although for other equivalence ratios there is a temperature increase below 400 K for the same distance covered. After that, the moderate temperature increase is observed up to the point x = 300 mm followed by a temperature plateau until the combustion chamber outlet.

The O_2 concentration profiles of the CH_4/NH_3 mixtures behave similarly to the O_2 concentration profile obtained in CH_4, see figure

fuel-rich conditions, the O_2 concentration at the exit will be zero.

According to the CO_2 concentration present in figure 4, it can be seen that the CO_2 emission increases with the equivalence ratio up to the φ = 1. This happens because the onset of CO to CO_2 conversion occurs in a region close to the combustion chamber outlet, typically for x ≥ 400 mm, which causes an appreciable CO concentration at the combustor outlet.

The NO_x concentration data in figure 4 shows that for φ < 1 there is a higher tendency for NH_3 to oxidize and form NO_x and that for x > 400 mm there is a significant increase in NO_x concentration since the CO and CH_4 promote the formation of a radical pool consisting essentially of O, H and OH that accelerate the reaction rates and favor the ammonia oxidation pathways [10]. For fuel-rich conditions, the NO_x

concentration is less than under fuel-lean conditions since NH_3 is more propense to undergo pyrolysis than to oxidize, with N_2 and H_2 being the pyrolysis products. The NO_x concentration decreases downstream of point x = 314 mm because the NO_x consumption rate is higher than the NO_x formation rate. The NOx consumption is done essentially through the following chemical reaction [11]:

$$NO + NH_2 \Leftrightarrow N_2 + H_2O$$

zero for φ ≥ 1. The NH_3 and H_2 concentrations, see figure 5, indicate that when the equivalence ratio increases, the time needed to dilute NH_3 and H_2 increases, especially in the first half of the combustion chamber. This lower dilution rate is due to the lower air jet velocity when the equivalence ratio increases. For φ = 1.2, there is an H_2 concentration increase in the second half of the combustion chamber. This phenomenon happens because the ammonia has a greater tendency to pyrolyze and from N_2

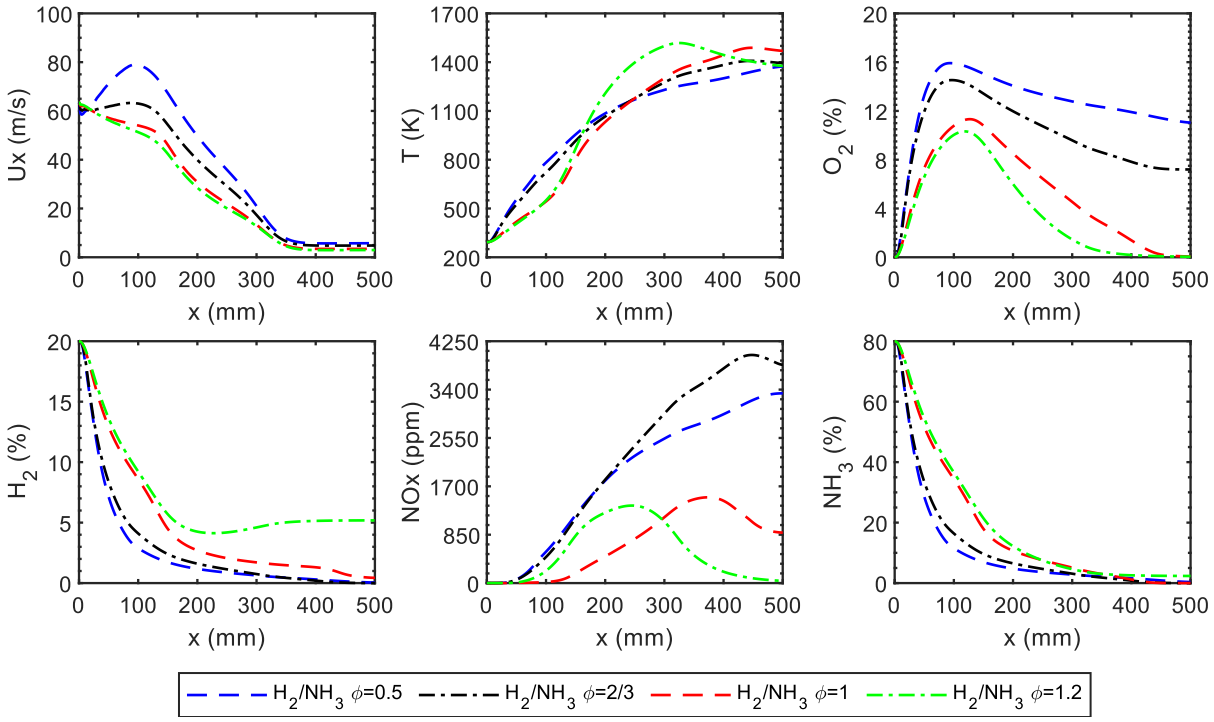

Figure 5 – Axial profiles of velocity, temperature, O_2, H_2, NO_x and NH_3 concentrations for combustion of H_2/NH_3 mixture.

From figure 5, it can be seen that the velocity profiles of the H_2/NH_3 mixtures have similar behavior to the velocity profiles of CH_4/NH_3 mixtures.

Regarding the O_2 concentration data, figure 5 shows that the O_2 concentration profiles of the studied H_2/NH_3 mixtures have the same tendency as the O_2 concentration profile in CH_4 combustion. As the equivalence ratio increases, the expected O_2 concentration at the combustor outlet chamber decreases and decreases to

and H_2 instead of oxidizing for fuel-rich conditions [10]. This H_2 concentration in the order of 5% is also present in the recirculation zones and near the wall.

At the combustor outlet, it is observed that for stoichiometric or fuel-rich conditions the NOx concentration is lower than the NO_x concentration presents in the fuel-lean conditions, see figure 5. For φ ≥ 1, the NO_x consumption occurs in the second half of the combustion chamber because the ammonia is

partially cracked after the heating period in which the NH_2 radicals are obtained. The NH_2 radicals react with NO to produce N_2 in lower temperature regions [12].

In figure 5, it is observed that in fuel-lean conditions, NO_x concentration is lower for φ = 2/3 than for φ = 0.5. This happens because for the condition φ = 2/3 there is a higher NH_3 to NO_x conversion due to the higher concentration of the radicals O, H and OH in relation to the last condition. For this reason, at the combustor outlet, the condition φ = 2/3 emits only 0.0016% H_2 and 0.0014% NH_3 compared to 0.036% H_2 and 0.296% NH_3 emitted in the condition φ = 0.5.

3.2 Flue Gas Emissions

The flue gas concentration for each fuel studied is presented.

The CO_2 concentration is less than 12% for any fuel tested although methane and biogas emit more than 100 ppm of CO, see table 3. The high CO content in biogas is due to the fact that biogas has a significant CO_2 concentration in its composition, which tends to act as an oxidizing agent in environments of higher temperatures. In both fuels, the reaction zone starts beyond the point x = 300 mm, which means that the combustion chamber is not long enough for total oxidation of CO.

Table 3 – Flue gas emissions on a dry molar basis for nitrogen-free fuels.

Fuel	Flue gas emissions		
	CO_2 (%)	***CO (ppm)***	***NO_x (ppm)***
CH_4	5.8	138.9	1.4
Biogas	9.0	228.7	1.1
Ethanol	7.3	93.5	14.9
Syngas	11.5	34.9	7.8

According to the NOx emissions in table 3, the ethanol combustion emits about 15 ppm of NO_x, while syngas emits around 8 ppm of NO_x and the remaining fuels emit less than 2 ppm of NO_x. According to Bal [13], the responsible NO_x formation mechanisms in flameless combustion are the thermal-NO and intermediate N_2O-route mechanisms, although the temperature range recorded in this work is less than 1800 K, which is the minimum temperature at which the thermal-NO mechanism has an expressive response. Based on this, it is expected that the contribution of the thermal-NO mechanism in the NO_x formation will be higher in the syngas combustion than in the other fuels since syngas combustion exhibits higher temperatures.

Based on the temperature and concentration profiles analyzed above and with the NO_x concentration in exhaust gas shown in table 3, the flameless combustion is characterized by NO_x emissions lower than 15 ppm for carbon-based fuels.

Table 4 – Flue gas emissions on a dry molar basis for different equivalence ratios for the CH_4/NH_3 mixture studied.

φ	Flue gas emissions				
	CO_2 (%)	**CO (ppm)**	**NO_x (ppm)**	**UHC (ppm)**	**NH_3 (ppm)**
0.5	2.1	607.8	3917.3	7.6	63.3
2/3	3.0	122.9	3658.5	0.3	2.8
1.0	4.4	1247.9	1682.7	0.2	4.1
1.2	3.2	12471.4	89.7	658.5	≈ 2.0%

For φ ≤ 1, the CH_4/NH_3 mixtures show a higher CO concentration (see table 4) because the beginning of the CO oxidation is close to the combustor outlet, which means that the combustion chamber is not long enough to promote the total oxidation of CO. In the fuel-rich condition, oxygen is not enough to

complete combustion of the CH_4/NH_3 mixture, which promotes high CO and fuel emissions despite low NO_x emissions.

Table 5 – Flue gas emissions on a dry molar basis for different equivalence ratios for the H_2/NH_3 mixture studied.

φ	Flue gas emissions		
	NO_x (ppm)	**NH_3 (ppm)**	**H_2 (ppm)**
0.5	3266.8	357.8	2956.0
2/3	3782.8	16.7	14.1
1.0	867.9	3968.3	1.0
1.2	34.2	≈ 5.2%	≈ 2.4%

The CH_4/NH_3 and H_2/NH_3 mixtures have low NO_x emissions in fuel-rich conditions (see tables 4 and 5) because ammonia, in oxygen-poor environments, tends to pyrolyze and form N_2 and H_2 and also the NO_x consumption that is associated to recombination of NO with NH_2 radicals. For this reason, the H_2/NH_3 mixture presents a concentration of H_2 in order of 5% despite its reactivity, see table 5.

Finally, flameless combustion of CH_4/NH_3 and H_2/NH_3 mixtures is expected to be possible with this combustor. However, it is necessary to confirm this hypothesis with experimental results and optimize this small-scale combustor in order to reduce NO_x emissions to make ammonia flameless combustion a viable alternative to flameless combustion of carbon fuels.

4. Conclusions

The numerical simulations of a small-scale combustor operating in a flameless combustion mode have been conducted. The main objective of this work was to study the flexibility of this combustor to burn different fuels in order to obtain the flameless combustion mode. All fuels were simulated and only methane provided essential experimental data for the validation of the turbulence, species transport and radiation models. The main conclusions of the results presented are as follows:

• The flameless combustion is expected to be performed on biogas and ethanol. In the combustor outlet, the NO_x emissions are below 2.5 ppm for biogas and ethanol emits 15 ppm of NO_x. The CO concentration is below 100 ppm except for the biogas, which the CO emission is above 200 ppm. This CO concentration increase in biogas occurs because the CO_2 in higher concentration in the fuel and at higher temperatures behaves as an oxidizing agent.

• Syngas is the fuel where the flameless combustion mode is not achieved. However, CO and NOx emissions are less than 40 ppm and 10 ppm, respectively. This result suggests that the combustor can perform conventional non-premixed combustion with lower CO and NO_x concentrations due to a strong flue gas recirculation rate.

• In CH_4/NH_3 mixtures, the flameless combustion is expected to be possible at $\varphi \leq 1$. In fuel-lean conditions, the NOx and CO emissions are higher than 3400 ppm and 120 ppm, respectively, and that for $\varphi \geq 1$ the CO emission is above 1200 ppm and the NO_x emission is below 1700 ppm. The NO_x emission decreases for $\varphi \geq 1$ because the NH_3 has a greater tendency to pyrolyze and form N_2 and H_2 and also due to the NH_2 and NO recombination to form N_2 and H_2O.

• In relation to H_2/NH_3 mixtures, the flameless combustion is expected to occur for $\varphi \leq 1$ and the NO_x emission is higher than 3000 ppm. In the fuel-rich condition, the conventional non-

premixed combustion is observed and the NO_x emission is below 1000 ppm.

• In the CH_4/NH_3 and H_2/NH_3 combustion, the CO, H_2 and NH_3 emissions in the exhaust gas suggest that the combustion chamber used is not long enough. The possible techniques to reduce the CO and NO_x emissions are the use of a larger combustion chamber, the external recirculation of the exhaust gases and the introduction of secondary air downstream of the second half of the combustor.

References

[1] "The Paris Agreement | UNFCCC." Accessed on Jan. 10,2020. [Online]. Available: https://unfccc.int/process-and-meetings/the-paris-agreement/the-paris-agreement. [Accessed: 16-Jan-2020].

[2] P. F. Li et al., "Progress and recent trend in MILD combustion," Sci. China Technol. Sci., vol. 54, no. 2, pp. 255–269, 2011.

[3] S. E. Hosseini and M. A. Wahid, "Biogas utilization: Experimental investigation on biogas flameless combustion in lab-scale furnace," Energy Convers. Manag., vol. 74, pp. 426–432, 2013.

[4] M. M. Huang et al., "Effect of fuel injection velocity on MILD combustion of syngas in the axially-staged combustor," Appl. Therm. Eng., vol. 66, no. 1–2, pp. 485–492, 2014.

[5] J. Ye, P. R. Medwell, E. Varea, S. Kruse, B. B. Dally, and H. G. Pitsch, "An experimental study on MILD combustion of prevaporised liquid fuels," Appl. Energy, vol. 151, pp. 93–101, 2015.

[6] G. Sorrentino, P. Sabia, P. Bozza, R. Ragucci, and M. de Joannon, "Low-NOx conversion of pure ammonia in a cyclonic burner under locally diluted and preheated conditions," Appl. Energy, vol. 254, pp. 1–7, 2019.

[7] A. Rebola, M. Costa, and P. J. Coelho, "Experimental evaluation of the performance of a flameless combustor," Appl. Therm. Eng., vol. 50, no. 1, pp. 805–815, 2013.

[8] A. Rebola, P. J. Coelho, and M. Costa, "Assessment of the performance of several turbulence and combustion models in the numerical simulation of a flameless combustor," Combust. Sci. Technol., vol. 185, no. 4, pp. 600–626, 2013.

[9] Ansys Inc., Ansys Fluent Theory Guide, no. August. 2017.

[10] J. O. L. Wendt and C. V. Sternling, "Effect of Ammonia in Gaseous Fuels on Nitrogen Oxide Emissions," J. Air Pollut. Control Assoc., vol. 24, no. 11, pp. 1055–1058, 1974.

[11] S. Koger and H. Bockhorn, "NOx formation from ammonia, hydrogen cyanide, pyrrole, and caprolactam under incinerator conditions," Proc. Combust. Inst., vol. 30, no. 1, pp. 1201–1209, 2005.

[12] N. A. Hussein, A. Valera-Medina, and A. S. Alsaegh, "Ammonia- hydrogen combustion in a swirl burner with reduction of NOx emissions," Energy Procedia, vol. 158, no. 2018, pp. 2305–2310, 2019.

[13] M. Bal, "Numerical investigation of the influence of operating conditions on a mild laboratory scale combustor," Master Thesis in Energy Engineering and Management, Instituto Superior Técnico, Universidade de Lisboa, 2015.